THE JOURNAL OF PHYSICAL CHEMISTRY B
A JOURNAL OF THE AMERICAN CHEMICAL SOCIETY

pubs.acs.org/JPCB

Article

Occupancy Analysis of Water Molecules inside Channels within 25 Å Radius of the Oxygen-Evolving Center of Photosystem II in Molecular Dynamics Simulations

Divya Kaur,* Krystle Reiss, Jimin Wang, Victor S. Batista, Gary W. Brudvig, and M. R. Gunner

Cite This: https://doi.org/10.1021/acs.jpcb.3c05367

Read Online

ACCESS | Metrics & More | Article Recommendations | Supporting Information

ABSTRACT: At room temperature and neutral pH, the oxygen-evolving center (OEC) of photosystem II (PSII) catalyzes water oxidation. During this process, oxygen is released from the OEC, while substrate waters are delivered to the OEC and protons are passed from the OEC to the lumen through water channels known as the narrow or the O4 channel, broad or the Cl1 channel, and large or the O1 channel. Protein residues lining the surfaces of these channels play a critical role in stabilizing the hydrogen-bonding networks that assist in the process. We carried out an occupancy analysis to better understand the structural and possible substrate water dynamics in full PSII monomer molecular dynamics (MD) trajectories in both the S_1 and S_2 states. We find that the equilibrated positions of water molecules derived from MD-derived electron density maps largely match the experimentally observed positions in crystallography. Furthermore, the occupancy reduction in MD simulations of some water molecules inside the single-filed narrow channel also correlates well with the crystallographic data during a structural transition when the S_1 state of the OEC advances to the S_2 state. The overall reduced occupancies of water molecules are the source of their "vacancy-hopping" dynamic nature inside these channels, unlike water molecules inside an ice lattice where all water molecules have a fixed unit occupancy. We propose on the basis of findings in our structural and molecular dynamics analysis that the water molecule occupying a pocket formed by D1-D61, D1-S169, and O4 of the OEC could be the last steppingstone to enter into the OEC and that the broad channel may be favored for proton transfer.

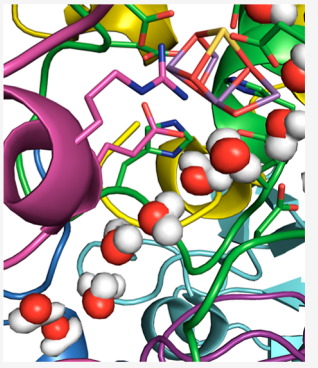

INTRODUCTION

Photosystem II (PSII) is a water-plastoquinone oxidoreductase enzyme catalyzing the oxidation of water upon light absorption.[1] The PSII structure is a homodimeric protein complex (700 kDa) embedded in the thylakoid membrane of cyanobacteria, algae, and higher plants (Figure 1A).[2] Each PSII monomer has approximately 20 protein subunits with bound cofactors for light absorption and electron transfer reactions. PSII uses water as the terminal electron donor, producing O_2 as the product, inside the oxygen-evolving center (OEC) , with an inorganic Mn_4CaO_5 cluster as the catalyst (Figure 1A).

Oxidizing water to O_2 is a thermodynamically unfavorable, uphill reaction, which the OEC carries out at room temperature and physiological pH several hundred times per second upon the absorption of photons.[3,4] The OEC is a unique catalyst in biology,[2] with few connections to other biological catalysts. The region around the OEC is highly conserved from cyanobacteria to higher plants.[5] The OEC is well buried inside a hydrophilic pocket on the lumenal side of PSII with controlled access of water molecule substrates and product oxygen as well as proton release through long water channels to the protein surface.

In PSII, light absorption initiates a series of electron transfer reactions starting with a charge separation at the P_{680} chlorophylls on the lumenal side, reducing quinones that lie on the stromal side of the membrane-embedded protein.[6−8] The OEC reduces P_{680}^+, via Tyr Z (Y_Z), following each PSII excitation. The production of each O_2 removes four electrons from two water molecules, requiring four photon absorption events. The OEC first accumulates four oxidizing equivalents, cycling through the five S states.[9−11] When the OEC has lost four electrons, in a transient S_4 state, the two water molecules are oxidized in the step leaving the OEC in the S_0 state gaining four more electrons. Protons from the OEC or from bound, substrate waters are transferred to the lumen, with one lost on each of the $S_0 \rightarrow S_1$ and $S_2 \rightarrow S_3$ transitions and two protons lost in the $S_4 \rightarrow S_0$ transition.[12,13] The protons released into the lumen add to the proton gradient that fuels ATP synthesis in F_1/F_0 ATPase.[14]

Water must travel into and protons out of the OEC, which is buried ≈20 Å from the surface. Analysis of the structure of the water networks in cyanobacteria shows that near the OEC water molecules form an interconnected network.[15,16] Three,

Received: August 8, 2023
Revised: January 29, 2024
Accepted: January 30, 2024

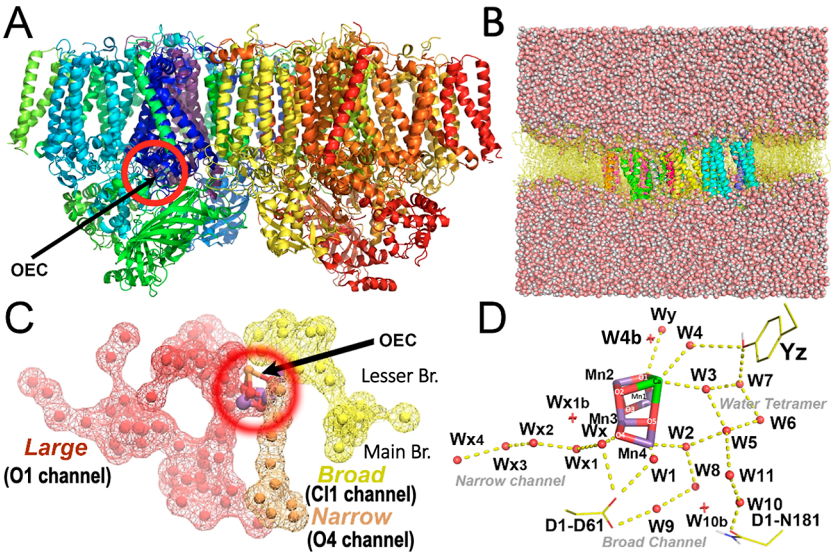

Figure 1. Overall PSII structure, MD simulation box, and water channels. (A) Overall PSII structure is colored by subunits. The circle shows the location of the OEC. (B) MD is the setup of a PSII monomer (subunits A−Z) embedded in a lipid membrane and surrounded by a 180 Å × 180 Å × 81 Å rectangular water box. (C) OEC is surrounded by three water channels: the narrow (O4 channel), the broad (Cl1 channel), and the large (O1 channel). The narrow channel (orange) extends from O4, and the broad channel (yellow) extends from O5 and W2 and is curved between D1-D61 and D2-K317. The large channel (red) extends from the channel of O1 and is the widest of the three channels. As shown previously,[15] the water channels are interconnected near the OEC. Main and lesser branches are also labeled. (D) Aqueous hydrogen-bonding network within 10 Å of the OEC: water molecules are shown as red spheres, the OEC as thick sticks (Mn: purple, O: red, and Ca: green), and amino acids as thin yellow sticks. Dotted yellow lines indicate probable hydrogen bonds (O−O distances of ∼3 Å or less). Alternate water positions are shown as crosses and have a "b″ added to their names. There are 10 named water molecules used in this study in the region surrounding the OEC. These are W1−W9 and W_X. Additional water molecules that are highly conserved across all high-resolution PSII structures include the first four water molecules after W_X in the narrow channel (W_{X1}−W_{X4}), the two water molecules near Oδ1 of N181 (W10 and W11), and the water molecule hydrogen-bonded to O1 (W_Y).

well-studied water channels denoted as O4 channel or narrow channel, Cl1 channel or broad channel, and O1 channel or large channel can be traced moving away from the OEC.[2,15−20]

The narrow channel (O4 channel) is connected to the O4 μ-oxo of OEC and extends to the lumen at the interface of the PsbO/PsbU subunits.[2,20] Several studies support this channel as the proton exit during the S_0-to-S_1 transition.[21−23] The single-file arrangement of water molecules inside this channel around the OEC also makes it a perfect channel for the substrate water delivery,[17] which must be selective for the water substrate. The broad channel (Cl1 channel) connects to the OEC near O5 and extends to the lumen via the PsbO subunit.[2,20] Recent MD studies[15,23] and X-ray crystal structures[18] favored this channel for proton exit due to the formation of a long-range extensive hydrogen-bonding network connected to the lumen.[23,24] Calculations found that the free energy for the formation of a possible hydronium ion was at the lowest inside the broad channel, especially near the exit to the lumen.[15]

The large channel (O1 channel) connects to the OEC near O1 and extends to the lumen via the PsbV subunit. Computational MD studies[15] and X-ray structures[23] found this channel to be hydrophobic with a less connected hydrogen-bonding network, so it may not be suitable as a proton exit pathway. Other studies found that this channel could also be a plausible pathway for the substrate water delivery.[18,25−28] However, a high-resolution cryo-EM structure of PSII from *Synechocystis* sp. PCC 6803 found that this channel is not conserved among different species of cyanobacteria owing to a different binding of the PsbV subunit to PSII from *Synechocystis* compared to PSII from thermophilic cyanobacteria.[29] We cannot rule it out that this channel is a substrate supply channel, and if this is indeed so, new MD simulations using the *Synechocystis* structure are needed, which is beyond the scope of this study.

In this study, we examined the localization and exchange of water molecules within 25 Å of the OEC in MD trajectories in the S_1 and S_2 states. The present work computes the electron density maps or atomic probability density functions (PDFs), an analysis of occupancies, and the decay function for known water positions throughout the MD trajectories. The study provides key insights into the water transport and hydrogen-bonding network necessary to understand the structural water dynamics in the $S_1 \rightarrow S_2$ transition. The water positions from the MD simulations are further compared with the water molecules modeled in X-ray crystal structures.[18,23]

METHODS

Details of MD Simulations. The MD model was prepared starting with the high-resolution 1.9 Å X-ray structure PDB ID: 4UB6 of a PSII monomer of *Thermosynecoccus vulcanus* including all 20 subunits.[2] CHARMM-GUI[30] was used, which generated the bilayer membrane via a bilayer membrane builder and the water box to set up the system (Figure 1B). The ionization states of acidic and basic residues were modified based on Multi Conformation Continuum Electrostatics (MCCE) calculations of the protein in the S_1 and S_2 OEC redox states at pH 6.5, with all other cofactors in their ground state.[31] All Asp, Glu, Arg, and Lys are ionized, and His, Cys, and Tyr are neutral with the following exceptions: CP47-D380, E387, E405, CP43-E413, D2-E242, E343, PsbO-D102, D224, E97, PsbV-K47, and K134 are neutral, while His D1-

https://doi.org/10.1021/acs.jpcb.3c05367
J. Phys. Chem. B XXXX, XXX, XXX−XXX

H92, H304, H337, CP47-H343, CP43-H74, H398, PsbO-H228, and PsbU-H81 are protonated. In addition, by default, CHARMM-GUI chooses neutral His with a proton on ND1 (HSD). However, MCCE found that the following His residues prefer to have a proton on NE2 (HSE): D1-H195, H252, CP43-H157, H201, D2-H61, H87, H189, H336, PsbO-H231, and PsbV-H118.[15] The details of all the parameters of cofactors[15,32] and RESP charges of the OEC (Table 1) were included.[15,32,33] Nonstandard protonation states were added with CHARMM-GUI.[15] The trajectories were obtained for both the S_1 and S_2 states of the OEC (Figure 2) using OpenMM[34] and were described in detail by Kaur et al.[15] All of the production runs were 100 ns long.

Table 1. Partial Charges for the OEC in the S_1 and S_2 States[a]

atom	S_1	S_2
Ca	1.518360	1.395880
Mn1	1.204720	1.193870
Mn2	1.194920	1.244060
Mn3	1.664330	1.520380
Mn4	1.518050	1.397600
O1	−0.705061	−0.675102
O2	−0.655159	−0.613125
O3	−0.759029	−0.752491
O4	−0.763103	−0.639714
O5	−1.007389	−0.903511

[a]Note that much of the increased charge in the OEC is absorbed by the water and protein ligands.

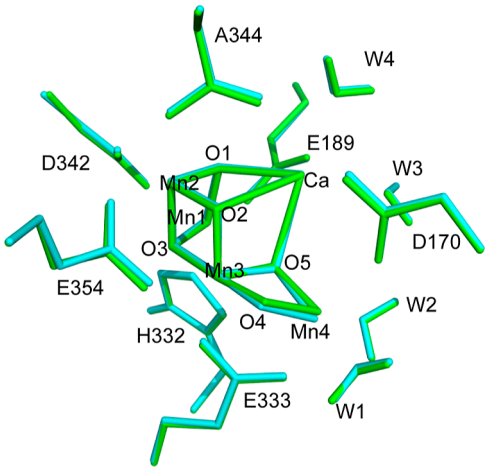

Figure 2. Overlay of S_1 (green) and S_2 (cyan). The difference between these structures is very slight, mostly contained to O4 and Mn4.

Occupancy Analysis. The occupancy of individual water positions was determined from the analysis of the final 50 ns of the S_1- and S_2-state full PSII monomer simulations. A total of 12,500 snapshots were combined into a single structure, which was then used to simulate a PDF using a unit scattering factor (such as a neutron scattering factor) using the SFALL program[35−37] within the CCP4 software package,[38] as described elsewhere.[39−43] A sample CCP4 code is given in the Supporting Information.[33] All hydrogens were renamed as deuterons for enabling the use of the neutron scattering library without a change in their positions (one could modify the neutron scattering factor in the library to make H atoms have a unit scattering value). The oxygen positions of all water molecules, including the ligand water molecules, within 25 Å of the OEC were identified. An 80 $Å^3$ spherical map was created with a resolution of 3 points/Å. PyMOL[44] was used to visualize the generated maps at a variety of contouring levels to determine which water positions were the most consistent throughout the trajectories.

When the X-ray form factor $f(s)$ is used for Fourier transformation of coordinates in each frame and for the summation of all images, the resulting electron density peak follows the following multiple Gaussian equations in the polar coordinate system, which can be simplified by a single Gaussian function under the condition when the atomic B-factor of root-measure squares of atomic fluctuation is much larger than those of the intrinsic atomic electron density distribution.[45]

$$\rho(r) = q\int f(s)\mathrm{d}\tau = 8\pi^{3/2}q\sum_{j=1}^{5}\frac{a_j e^{-4\pi^2|r|^2/(B+b_j)}}{(B+b_j)^{3/2}} \approx 8\pi^{3/2}e^{-4\pi^2|r|^2/B}/B^{3/2}q\sum_{j=1}^{5}a_j$$

where a_j and b_j are the Gaussian parameters of form factors and q is the occupancy. When the unitary form factor (i.e., neutron form factor) is used for analysis, the resulting PDFs follow exactly the single Gaussian function equation without any approximation or involve multiple Gaussian functions of the X-ray form factor. With or without approximation, the logarithm of the $r(r)/r(0)$ ratio is a function of r^2, independent of q, which is a function of the intercept of the straight line in the logarithm of $r(r)$ as a function of r^2.

Custom source codes were used to quantify the occupancy of the water positions in the trajectory.[33] To begin, the location of the center of each distinct water oxygen position was found visually based on the high-contour regions of the water maps and then refined using the Real Space Refine Zone tool in Coot.[46] The center coordinates of water molecules near the OEC identified as W1−W11, W_X, W_{X1}−W_{X4}, and W_Y and nearby alternate positions were determined in Coot. Probability densities and logarithmic decays as distance squares were calculated by averaging the map density along 12 evenly spaced vectors, which form a dodecahedron centered at the initial coordinates for generating data in the polar coordinate system using in-house scripts provided in the Supporting Information, Section S2.[33,47,48] Site occupancies were analyzed in Matlab.[49] A sample Matlab code is given in the Supporting Information, Section S3.[33]

RESULTS

Although the whole analysis is based on the last 50 ns from the 100 ns trajectories, the reported observations on hydrogen bonding and water occupancy shown are compared with the crystallographically derived maps for the water positions explained below and are in agreement with them.

Hydrogen Bonding of W1−W4, W_X, and W_Y near the OEC. The six water molecules that make direct contact with the OEC are designated as being "near-OEC" (Figure 1D).

https://doi.org/10.1021/acs.jpcb.3c05367
J. Phys. Chem. B XXXX, XXX, XXX−XXX

The four water molecules that are OEC terminal ligands are as follows: W1 and W2 coordinated to Mn4 and W3 and W4 bound to Ca^{2+}; and two other hydrogen-bonded water molecules are: W_X hydrogen bonded to O4 and W_Y to O1 (Figure 1D). The W1, W2, W3, and W4 terminal ligands were tightly bound to Mn4 and Ca of the OEC throughout the MD trajectory.[15] W_X and W_Y were free to move but only loosely restrained by nonbonding interactions. W_X accepts hydrogen bonds from D1-S169 and another water molecule, and it donates hydrogen bonds to O4 and D1-D61. In contrast, W_Y interacts only with O1 and other water molecules in the large channel, having no protein contacts. The locations of all water molecules in the channels, within 10 Å of the OEC, and their potential hydrogen-bond connections are shown in Figure 1D.

Table 2 summarizes the occupancies of all the water molecules within 10 Å of the OEC, in which occupancy was defined from cumulative counting through Fourier transformation when the oxygen of water molecules remained within 1.5 Å of a given equilibrium position for any water, as shown in Figure 1D, in either the S_1- or S_2-state MD trajectories. Figure 3 shows the relative probability of the oxygen sampling space away from the central, highest probability position in the S_1 state (Rows A and B) and the S_2 state (C and D), the probability density function (PDF) (Rows A and C), and the logarithm of the probability (Rows B and D). The columns separate the water molecules showing the OEC and W_X and W_Y (left panel), water molecules in the narrow channel (center panel), and water molecules in the broad channel (right panel). The PDF (A and C) shows the percentage of simulation frames in which a water molecule is present within a 1.5 Å radius of the center of the water position, measured in 0.05 Å increments. The log function quantifies how the probability decays with distance squared (or distance). This makes the comparison of the density size of the region occupied by a water molecule much easier, particularly when two positions have drastically different occupancies.

Table 2. Occupancies of Selected Water Molecules in the Narrow and Broad Channels and within the Y_Z Water Tetramer in the S_1 and S_2 States[a]

water	S_1	S_2	water	S_1	S_2
W1	1.00	0.97	W_X	0.94	0.91
W2	0.98	0.96	W_{X1}	0.81	0.12/0.60[b]
W3	0.95	0.95	W_{X2}	0.84	0.70
W4	0.92	0.93/0.19[b]	W_{X3}	0.80	0.32/0.56[b]
W5	0.83	0.76	W_{X4}	0.59	0.59
W6	0.28	0.60	W_{X3c}		0.61
W7	0.29	0.53	W_Y	0.42	0.31
W8	0.70	0.69	W10	0.45	0.23/0.38[b]
W9	0.88	0.81	W11	0.64	0.50

[a]The values are the integration of the water probability within 1.5 Å of the site center, as described in Figure 4, which provides relative occupancies. [b]Sites have been split into two closely related sites. When the summed occupancy is greater than 1, which has only one single instance of W4 and W4b, the two split sites are considered to be mutually exclusive.

For example, in the S_2 state, both W_Y (red line) and W4b (cyan dots) had relatively low occupancies, but the radius over which the W4b position extended was much narrower, compared to that of the higher occupancy water molecules, whereas the W_Y position spread over a larger area. More dynamic water molecules surrounding their equilibrium positions have larger root-mean-square fluctuations or larger atomic *B*-factors than less dynamic water molecules, which are visualized in the slopes of the logarithm plots. The reduction of occupancy does not change the slope but reduces the intercept of the plot. Three-dimensional integration of the PDF would result in the total number of atom numbers (or total electron number if X-ray scattering factors for Fourier transformation) near the given equilibrium position, which could be converted to relative occupancy when compared with the expected numbers throughout the MD trajectories.[47,48]

The four OEC terminal ligands show a slight decrease in the integrated occupancy, with W1 always present, while W4 has an integrated occupancy of only 0.92 (Table 2). W3 and W4 form longer bonds (~2.5 Å) with Ca^{2+} compared with those of W1 and W2 (~2.0 Å) to Mn4. The extra 0.5 Å bond length of W3 and W4 gives them a wider range of motion. Thus, these water molecules can sometimes move outside of the defined 1.5 Å radius, due to an independent motion of the individual water or due to a collective rigid-body motion of the entire OEC.

The atomic motion of W4 was not purely spherically symmetric. It could be divided into two closely related equilibrium positions, the original W4 and a new W4b position, as shown in Figure 1D. This new W4b occasionally appeared in MD trajectories, 2.7 Å from W4 and 2.6 Å from the Ca^{2+}, but only present in part of the S_2-state trajectory. The corresponding occupancies of W4 and W4b were 0.93 and 0.19, respectively. The sum of the two values was greater than 1, suggesting that the two positions were not fully and mutually exclusive. They could be two partially independent water molecules next to Ca^{2+} with limited exclusion of each other (Table 2). When the two water molecules were simultaneously present in the W4 and W4b positions, they could still form a short hydrogen bond with each other. Interestingly, W4b was not seen in the S_1-state trajectory, perhaps related to the reduced charge for this state of the OEC relative to the S_2 state. Due to its low occupancy, the hydrogen atoms of W4b could not be visualized in the full water map when H (or D) atoms were included in the analysis, even at very low contour levels. Therefore, the current analysis could not provide information about the orientation of the water molecule occupying the W4b position. This low probability position was not well documented in any of the 1F PSII crystal structures.[50] It is interesting to note that in the monomer B of both the 4UB6/0F and 4UB8/0F structures, the Ca^{2+} ion of the OEC has an extra terminal ligand that is very close to this W4b position,[51] raising a possibility that monomer B in these structures may contain some fraction of the S_2 state.

The other two nonligand water molecules near the OEC were W_X and W_Y, which had some unique characteristics. Unexpectedly, W_X had an occupancy on par with the ligand water molecules (Table 2), even though it did not appear to make any stable hydrogen bonds with the nearby protein partners. This water molecule sat in the center of the pocket formed by three rigid groups of O4, D1-D61, and D1-S169, forming hydrogen bonding with them but did not appear to have a large atomic motion. The rigidity of these residues can be seen in the additional hydrogen bonds they make with other protein residues, i.e., D1-D61 with W1 and D1-S169 with D1-S167. These environments made the W_X position into a high-affinity site that was as stable as the terminal ligand water molecules of the OEC. The stability is likely to be contributed

https://doi.org/10.1021/acs.jpcb.3c05367
J. Phys. Chem. B XXXX, XXX, XXX−XXX

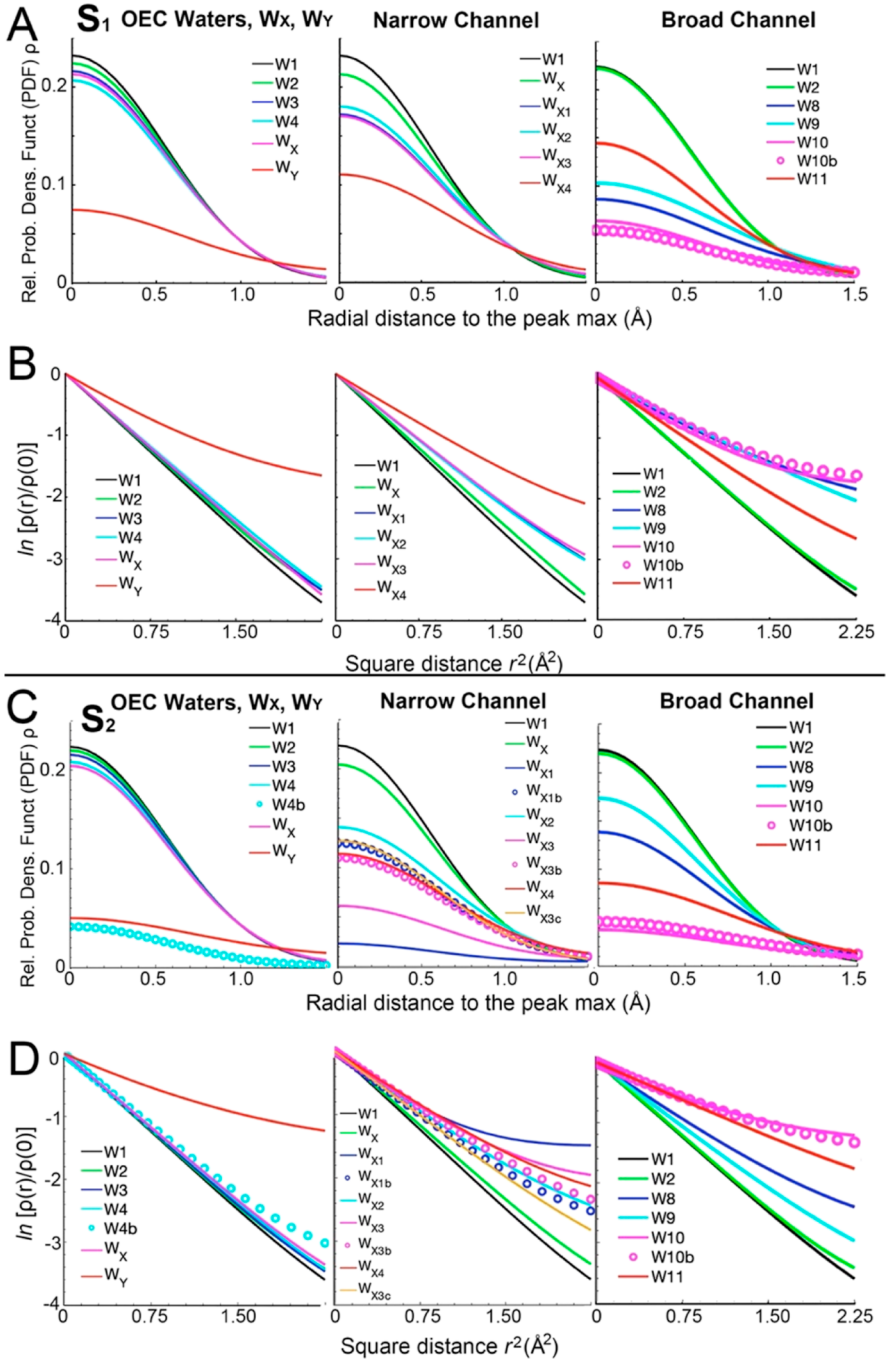

Figure 3. Probability density function (PDF) and occupancy analysis of water molecules. A and B are the relative probability density and logarithmic function plots in the S_1 state as functions of distance (on the same scale), while C and D are the relative probability density and logarithmic function plots in the S_2 state (on the same scale). Left panel shows the OEC waters, W_X and W_Y. Center panel shows the water molecules in the narrow channel, while the right panel shows the water molecules in the broad channel.

by some electrostatic potential interactions to compensate for missing hydrogen bonds as well as the orientations of lone-pair electrons and hydrogen atoms. This water molecule-binding pocket (host) is made by hydrophilic residues and the OEC. However, the existing hydrogen-bonding network among protein residues forms a rigid cage-like host cavity that is not suitable for making specific hydrogen bonds with this water molecule while making some electrostatic host−guest interactions.

In our full PSII monomer MD model, all water molecules could, in theory, freely move in and out of the channels that run through the protein. Thus, despite being free and nonbounded, W_X did not appear to move or exchange with other water molecules throughout the MD trajectory. Seeing this unusual MD property, we propose that water W_X is a waiting-inline queued substrate water molecule, which has already been isolated completely from the bulk solvent and stripped of all possible hydrogen bonds with the protein so that it is ready to enter the OEC. Without the baggage of any existing hydrogen bond, this substrate water can freely enter the OEC in the energetically downhill movement without the need to pay any energetic penalty once the OEC is further

https://doi.org/10.1021/acs.jpcb.3c05367
J. Phys. Chem. B XXXX, XXX, XXX−XXX

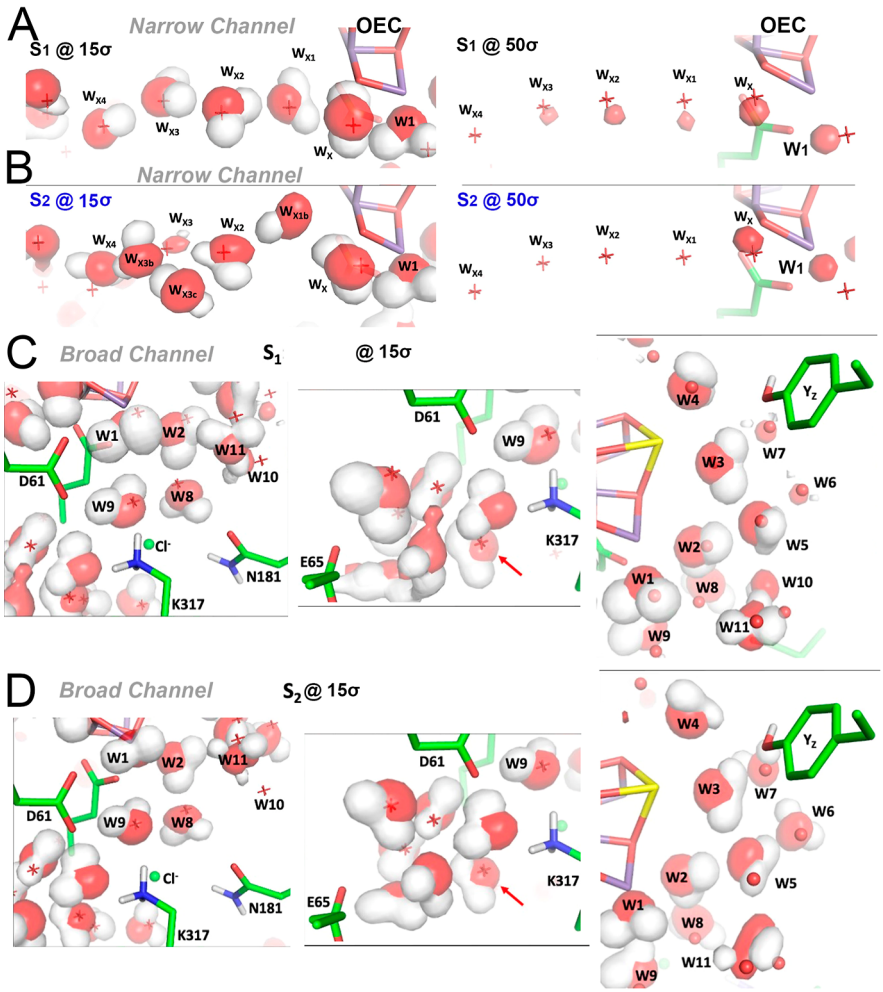

Figure 4. Visualization of water molecule occupancies inside narrow and broad channels. (A) Inside the narrow channel with the PDF maps contoured at 15σ (left panels) and 50σ (right panels) in the S_1 state. (B) S_2 state. MD-derived PDFs are shown in red surfaces, and the crystallographic water molecules found in 3WU2[2] are marked by crosses. In the S_1 state, the occupancy of W_X and the first three water molecules in the narrow channel persists even at very high levels of contouring. In the S_2 state, only W_X is visible at 50σ. (C) Inside the broad channel for S_1 MD simulations with PDF maps contoured at 15σ. (D) S_2 state. Key protein residues in the equilibrated positions of the MD simulations are also included for referencing water molecule positions. W8 and W9 mark the beginning of the channel (top left panels and a close-up view in middle panels), in which W9 serves as a barrier or a bridge between D61 and D2-K317. Bottom panels: the remaining water molecules in the broad channel have a distinct cluster of seven water molecules, which are three more than the crystallographically observed water molecules.[2,54]

oxidized. This water substrate could be part of the carousel mechanism proposed for the OEC during the 0F-to-2F transition.[50,52] One important point to note is that there were no experimental 1F data available at the time when the carousel mechanism was proposed.

W_Y is often overlooked in terms of the hydrogen-bonding network surrounding the OEC, partly because it had relatively poor experimental electron density and noticeably reduced occupancy in crystal structures, partially present in some structures and more often missing in other structures.[25,51,53,54] It marks the beginning of the large channel, which is the most dynamic of the three water channels. In our MD trajectories, W_Y has the poorest defined position of any of the near-OEC water molecules and lacks any specific interaction with the protein. Its only rigid contact is with the corresponding O1 of the OEC. Having an integrated occupancy of less than 0.5 (Table 2), unlike many other water molecules, as discussed below, W_Y does not have an obvious alternative position, so it may simply move in and out of the large channel inside a large and spatially defined area. This feature is fully consistent with X-Ray Free-Electron Laser (XFEL) crystal structures.[51] While other water molecules have an almost linear logarithmic decay, indicating they move with low probability away from the equilibrium position (Figure 3), W_Y falls off slowly, indicating it has a larger *B*-factor or rms fluctuation value around its equilibrium position in the probability plot, having a higher probability of being beyond ~1.25 Å, a property that is not found for any other water molecules. The exploration of space by W_Y is not directly related to its relatively low occupancy. This can be seen with the position distribution of the low-probability W4b, which has a distance dependence of position that is similar to other bound water molecules with only a slight deviation toward the far edge of the position. Thus, W_Y has the most loosely defined position of any of the near-OEC water molecules.

Water Molecules inside the Narrow Channel in the S_1 State. Figure 4A shows the most prevalent positions of the water molecules in the narrow channel. They include five well-isolated water positions (W_X, W_{X1}–W_{X4}) as seen near the OEC in the S_1 state, distributed gradually moving away from the

https://doi.org/10.1021/acs.jpcb.3c05367
J. Phys. Chem. B XXXX, XXX, XXX−XXX

OEC. The distribution of water molecules occupying these sites is almost perfectly spherically symmetric, which is similar to the distribution of water molecules in the W1−W4 binding sites that are terminal ligands to the OEC (Figure 4). These water positions in the narrow channel were found to perfectly align well with the experimentally observed positions in the crystal structures.[2] However, although one water is present in each of their assigned positions in most MD frames, the individual water molecules were rapidly interchanged throughout the simulation with the exception of W_X, as discussed above. Beyond W_{X4}, the individual water molecules of the narrow channel are no longer clearly distinguishable, as they are not well localized.

The five water molecules at the beginning of the narrow channel are sufficiently well localized so that all of the hydrogen positions can be visible in the analysis of the MD trajectories, forming a defined network of hydrogen bonds. The hydrogen positions are also almost perfectly spherical. W_X predominantly forms a hydrogen bond with O4 of the OEC. Proceeding down the narrow channel sequentially moving away from the OEC, the first four water molecules are pointed in the same direction, with their protons pointing toward the OEC (Figure 4A). W_{X1}, W_{X2}, and W_{X3} have a very distinctive pattern, each having one hydrogen pointed toward the OEC and the second pointed elsewhere. The second hydrogen atoms of these water molecules are locked onto a rigid donor−acceptor relationship with the hydrogen-bond acceptors from the protein, i.e., with those of CP43-E354-Oϵ2, D1-D61-O, and D1-A334-O for W_{X1}, W_{X2}, and W_{X3}, respectively. All of these are rigid acceptors, with E354-Oϵ2 also being a ligand to the OEC and the latter two being backbone atoms. Therefore, the oxidation state of the OEC could directly control or influence the dynamics of water molecules occupying these sites, as further demonstrated below.

The last of the water molecules in the linear chain, W_{X4}, appears to maintain the same spherical density distribution as its neighbors, despite not having any protein contacts and only participating in three hydrogen bonds with other water molecules in the narrow channel, one of those being W_{X3}. However, the quantitative analysis of occupancy reveals that this appearance of consistent stability is deceptive (Table 2). The other four linear water molecules have occupancies of at least 0.8, while W_{X4} drops to 0.6 (Table 2). Similarly, in Figure 4A, W_{X4} (red) has a less strictly defined position, like that of amorphous W_Y. This is not surprising, considering that both water molecules predominately form hydrogen bonds only with other mobile water molecules, yielding less well-defined positions. This observation suggests a "vacancy-hopping" mechanism for the dynamic movement of water molecules inside the single-file narrow channel and likely in all other channels. If all three consecutive single-filed water-binding pockets (i.e., W_{X1}, W_{X2}, and W_{X3}) are at full occupancy (q = 1.00), the water molecule occupying the middle site (W_{X2}) cannot move to either of its two flanking sites (W_{X1} and W_{X3}). The movement of this middle water requires some vacancy (or water "hole", not to be confused with oxidizing "hole") of its two flanking sites and can be described as a "vacancy-hopping" or "water hole"-hopping mechanism. We find that the occupancies of W_{X1}, W_{X2}, and W_{X3} in the S_1 state were about 0.80 to 0.84 (Table 2), providing the MD basis for the "vacancy-hopping" dynamics of water molecules occupying this channel. For a given functional state of protein, the protein provides specific binding sites for water molecules, where they can vary their occupancies depending on the hydration states and temperature. The occupation of water molecules can also modulate the protein dynamics, which can modify the binding pockets of water molecules as documented below in the S_2 state.

Water Molecules inside the Narrow Channel in the S_2 State. In our MD simulation, we find that when the OEC is oxidized into the S_2 state, there is a stark change in the properties of water molecules occupying the binding pockets inside the narrow channel (Figure 4B). In the S_1 state, water molecules have spherically symmetric distributions inside the narrow channel, as described above, but in the S_2 state, their distributions were smeared and squished, with the exception of W_X, which remained largely spherically symmetric as in the S_1 state (Figure 4B). The most prominent difference feature is that almost all water molecules inside the narrow channel have reduced occupancies in the S_2 state relative to those in the S_1 state in MD trajectories, with the exception of W_X (Table 2). We hypothesize that this would make sense if W_X has been aligned to be easily accepted by Mn4, and the rest of the channel is preparing to be shifted toward the OEC during the S_2−S_3 transition; future studies of the S_2−S_3 transition are needed to test this hypothesis. The most notable positional change is that W_{X1} has moved in addition to its reduced occupancy (Figure 4B).[19,26] However, in the S_1 state, it sits below W_X and W_{X2} interacting with CP43-E354-Oϵ2, and W_{X1} now primarily sits closer to CP43-R357 in the S_2 state. W_{X1} also has the largest occupancy reduction in addition to the displacement from q = 0.81 to q = 0.12 in the primary binding pocket and q = 0.60 in the nearby displaced site. The reduction can be visualized at the two contouring levels of the PDF, a low level of 15σ and a high level of 50σ (Figure 4B). At the high contouring level of 50σ, the PDF remains visible for W_{X1} to W_{X3} in the S_1 state but not in the S_2 state. At the low contouring level of 15σ, the PDF for these sites in the S_1 state remains spherically symmetric, but it becomes smeared in the S_2 state.

The apparent loss of occupancies in some binding pockets inside the narrow channel in the S_2 state is due to the splitting of these sites to multiple subsites. For example, two new water molecules (W_{X3b} and W_{X3c}) appeared near W_{X3} (Figure 4B), of which W_{X3b} is most likely an alternate position for W_{X3}. The summation of the occupancies of W_{X3} and W_{X3b}, which are 0.32 and 0.56 in S_2, respectively, adds up to 0.88, which is close to the original W_{X3} occupancy of 0.80 in the S_1 (Table 2). W_{X3b} retains roughly the same position in the narrow channel water chain, serving as a link between W_{X2} and W_{X4} in both S states. However, W_{X3c} has an occupancy of 0.61 in the S_2 state and thus is a new water molecule rather than an alternate position, as both water molecules are present in the same frames. The MD occupancy of these water molecules in the narrow channel is largely consistent with the crystallographic electron density maps for which only W_{X1} has lost significant occupancy,[27,54] whereas all other molecules inside this channel become more flexible in the S_2 state, resulting in a disorganized water network.

To understand how the MD trajectories underwent the large change in water reorganization during the $S_1 \rightarrow S_2$ transition, we examined the distribution of hydrogen atoms on each of the water molecules occupying major binding sites inside the narrow channel and found that they have different hydrogen-bonding networks in the two states. In the S_1 state, W_X is primarily hydrogen-bonded to the μ-oxo bridge of the OEC.

https://doi.org/10.1021/acs.jpcb.3c05367
J. Phys. Chem. B XXXX, XXX, XXX−XXX

However, when Mn4 is oxidized in the S_2 state, the change in charge is also distributed between Mn4's neighbors and thereby decreases the negative partial charge of O4 in the S_2 state relative to the S_1 state. This decreases the strength of the hydrogen bond between O4 and the hydrogen of W_X and thereby flips the hydrogen orientations of this water molecule, i.e., it then primarily donates its hydrogen bond to W_{X1}. This in turn causes the entire hydrogen-bond chain of the narrow channel to flip. This local increase in the charge of the OEC causes long-range ripple effects through water flipping of their hydrogen positions, which can be very fast and efficient on a very large scale, simultaneously for many water molecules. Whereas in the S_1 state, hydrogen bonds are donated toward the OEC, in the S_2 state, they now move away from the OEC. When this switching reaches W_{X3}, the distribution of water molecules occupying this water position becomes very destabilized, exhibiting a bimodal distribution. While a single-filed water network can be an efficient pathway for proton hopping, a branched pathway with destabilized water molecule-binding sites could better deal with an extra proton, i.e., more conducive to proton transport out of the cluster at the ending point of a proton exit pathway.

The new alternate position, W_{X3b} (Figure 4B), lies close to a nearby unnamed channel to form a short two-water bridge connecting the two branched channels via W_{X3c}. This new position has pushed the protein side chain CP43-Met356 out of the way, clearing the way for two water molecules to bridge the gap between two previously separated channels. Despite one of the bridging water molecules, W_{X3c}, having an occupancy of 0.6 and having clearly visible hydrogen positions, the second water W_{X3b} lies closer to the unnamed channel and is not readily identifiable in a discrete position. This second water molecule is barely visible at 7σ and appears oblong or with strong anisotropy in motional distribution, visible at further lowered contour levels. When an anisotropic distribution has large differences in tensors, it can typically be split into two positions, which are found to be only 1.5 Å apart for this peak. With the limited number of current MD frames, occupancy analysis for two such water positions that are so close to one another is no longer reliable. Nevertheless, we can still conclude with certainty that a water molecule occupying the W_{X3b} site is less stable and more transient than its interacting partner of W_{X3c}, even without any quantitative occupancy information. Therefore, this pair of water molecules, particularly the transient W_{X3b}, could serve as a gating mechanism for a water delivery pathway rather than as a proton exit pathway, for which the network is typically highly organized.[18,23]

The apparent changes of water molecules occupying the binding sites inside the narrow channel from the S_1 state to the S_2 state from the MD snapshots show interesting observations. In the S_1 state, the water molecules form a single-file network from O4, W_X, and W_{X1} to W_{X4} where the channel becomes broad and merged with another unnamed channel nearby. On the other hand, in the S_2 state, the branching point moves backward to W_{X2}, shortening the single-filed network by two water molecules.

Water Molecules Occupying Binding Pockets inside the Broad Channel. Figure 4C,D shows the equilibrium positions of the water molecules derived from our MD simulation in the broad channel, and Figure S1 shows the corresponding occupancy analysis for the water molecules W1, W2, and W8−W11 in the channel. The broad channel is another channel proposed for the proton egress pathway.[15,18,26] Though it lacks the linear water chain of the narrow channel, the broad channel is rigidly organized due to the presence of the charged residues lining the surface of this channel and a Cl^- anion. The channel begins at W8 and W9. The W8 binding site is formed by W2, N181, and the Cl^- anion (Figure 4C). The W9 binding site is made by W8, D1-D61, and D2-K317 (residues correspond to the D1 subunit in this study, unless otherwise explicitly stated). In combination with the chloride ion, W9 serves as an important barrier between D2-K317 and D1-D61, disrupting the formation of a salt bridge between them.[31,55,56]

Visualization of the occupancy maps in Figure 4C,D reveals that water molecules occupying several distinct water positions in the broad channel clearly are very stable, and their hydrogen equilibrium positions form a well-defined pattern of hydrogen-bonding interactions. The first such water molecule is at W8, which accepts a hydrogen bond from W2 in the highest frequency in the MD trajectories. If the terminal W2 ligand becomes an internal oxygen ligand of the OEC during the $S_2 \rightarrow S_3$ transition, this hydrogen bond could serve as the first step for removing the proton that was observed to proceed during the $S_2 \rightarrow S_3$ transition (Figure 4D).[11,50] In addition to W2, W8 also accepts a hydrogen bond from W9 and donates its two hydrogen bonds to both Oδ1 of N181 and the Cl^- anion. This is fully consistent with the water positions and distances seen in many PSII crystal structures[2,18,54] and in theoretical models.[15] In both of the S states in our MD simulations (Figure 4C,D), W9 sits between D1-D61 and D2-K317, donating a hydrogen bond to the former and accepting one from the latter. Once past the D61-K317 checkpoint or gating point, the broad channel widens into a highly organized network of the stable cluster of six to seven water molecules. Like water molecules occupying the W8 and W9 sites and many other water molecules inside the narrow channel, all water molecules occupying other positions of the broad channel are almost perfectly spherically symmetric, all having well-defined hydrogen equilibrium positions.

While the S_2-state water positions in the broad channel in our MD simulations have closely reproduced those observed in crystal structures,[51] some of S_1 water molecules in this channel do not, especially around the Cl^- site. In the S_1 state, we observed the movement of the Cl^- ion toward D1-D61 by 1 Å in addition to its position occupied by the new water W_{Cl}. This new water accepts a hydrogen bond from N181 as chloride did originally and donates a hydrogen bond to the shifted Cl^-, acting as a bridge between the now-separated anion and N181. This feature is not observed in PSII crystal structures.[51] The movement of chloride is likely an artifact of the simulation due to nonoptimized parameters for the Cl^- ion, and the protonation states of the nearby carboxylate residues need to be adjusted for our MD; therefore, the position of Cl^- is restrained in the MD simulation of the S_1 state. The protonation state of E65 is considered ionized in the S_1 and S_2 MD simulations based on previous studies.[15,31] In separate MD simulations done by our colleagues, the Cl^- ion remains very stable when D1-E65 and several other carboxylates nearby are protonated and also with the addition of a bond restraint between the O atom of D61 and Mn4. Remarkably, despite how far Cl^- moves, all the hydrogen-bond connections are fully maintained with one exception (i.e., the hydrogen bond with D1-N181), including those in direct contacts to D2-K317 and the backbone amide of the D1-E333, all of which are

https://doi.org/10.1021/acs.jpcb.3c05367
J. Phys. Chem. B XXXX, XXX, XXX−XXX

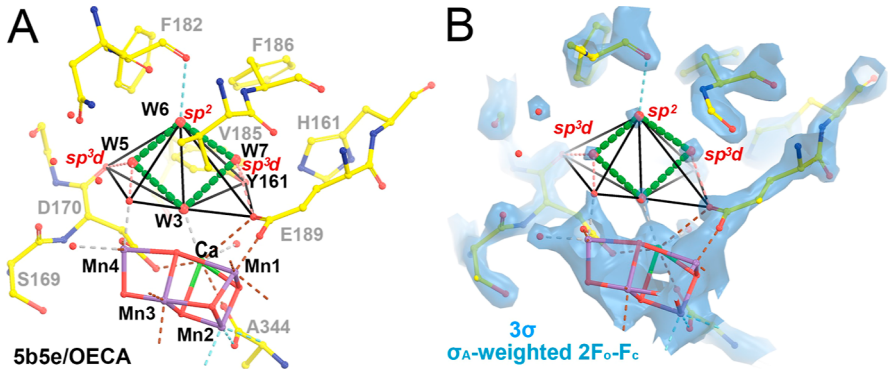

Figure 5. Geometry and environment of water tetramer (A) and retrieved σA-weighted 2Fo-Fc experimental map contoured at 3σ for the OEC of monomer A of the 5b5e/0F structure (B). Apparent atomic orbital hybridization of water molecules is indicated. Black lines indicate the trigonal pyramidal symmetry.

independent of the Cl^- shift. We note that the positively charged D2-K317 side chain is flexible to move as observed in many cryo-EM structures[57] and will retain a strong attraction to Cl^- directly or indirectly. However, under experimental conditions, the occupancies of metal ions inside the OEC-binding pocket were often found to be variables,[48] which could add another level of conformational variability in experimental structures but should not happen in our MD simulations. The maintained contact with the amide in the backbone of D1-E333 is somewhat unexpected, as it serves as a ligand to the OEC and is rigid but not strongly charged.

As we are interested in the MD properties of water in the broad channel when the Cl^- ion is in the X-ray position, we, therefore, fixed the Cl^- ion in the X-ray position, which also restored the crystallographically observed hydrogen bonds between W8 and Cl^- and W10 with N181. Both the S_1-state and S_2-state MD simulations show that water molecules occupying the major sites in the broad channel remain unchanged (Figure 4C,D). The occupancies of all water molecules inside the broad channel are less than those of the terminal ligand waters of the OEC and those of the water molecules in the narrow channel, regardless of which of the two MD simulations are analyzed, the S_1 state or the S_2 state (Table S1). W9 (hydrogen-bonded to W1, W8, D61, and D2-K317) has an occupancy >0.8 in both the S_1 and S_2 states. Given that W9 becomes a physical barrier to the formation of a salt bridge between D2-K317 and D61, its high occupancy is attributed to strong hydrogen bonds with two oppositely charged flanking residues of D61 and D2-K317. The W9 position could be a critical transit point for any proton egress through the broad channel by maintaining a stable hydrogen-bonding network that is needed to support a Grotthuss mechanism.[58]

Water Tetramer Next to Y_Z or D1-Y161. The water tetramer was initially identified in the first high-resolution crystal structure when water molecules began to be visualized in the crystallographic electron density maps[53] (Figure 1D). It forms a diamond shape with two acute angles (~75°) (W7 and W6) and two obtuse angles (~101−107°) (W3 and W5) with a cyclic head-to-tail donor−acceptor pattern of hydrogen-bonding interactions. An arrangement of four water molecules this way is very rare because the oxygen of a water molecule prefers to adopt sp^3 hybridization with a tetrahedral angle of 109.5° between its two hydrogen atoms and two lone pairs of electrons. With this sp^3 tetrahedral angle, the most commonly observed self-assembled water cluster is a water pentamer found on the surface of hydrophobic residues of many high-resolution protein structures including proline residues.[59] The interior angle of the pentagon is ~108°, which matches well with a tetrahedral angle of 109.5°. With such an acute angle of the oxygen atoms of W7 and W6, which do not have sp^3 hybrid orbital geometries in the unusual water tetramer in the OEC, there must be unusual underlying electronic structures. Instead, both oxygen atoms of W7 and W6 appear to adopt an approximately trigonal pyramidal geometry (i.e., sp^3d hybrid orbitals). Three equatorial interacting partners of W7 are D1-Y161Oh, Oε1 of D1-E189, and W5, and its apex partner is W3, which is also the apex interacting partner for the W6 atom (Figure 5). The three equatorial interacting partners of W6 are W3, W5, and the carbonyl group of D1-D170. In our MD simulations, we treated these four water molecules just like any other water molecule. It is likely that the energy parameters for these nonstandard water molecules are underestimated. Therefore, their dynamic properties could be overestimated, and their occupancy underestimated. Nonetheless, it is important to report what we have observed about this water tetramer in the current MD simulations under the standard conditions.

The PDFs of both oxygen and hydrogen atoms for the water tetramer are shown in Figure 6 and their occupancies are summarized in Table 2. First, the values of occupancies of water molecules in the water tetramer were quite low, which is not consistent with the crystallographic data.[51] We attribute this discrepancy to the unoptimized parameters for these water molecules. Second, during the $S_1 \rightarrow S_2$ transition, the

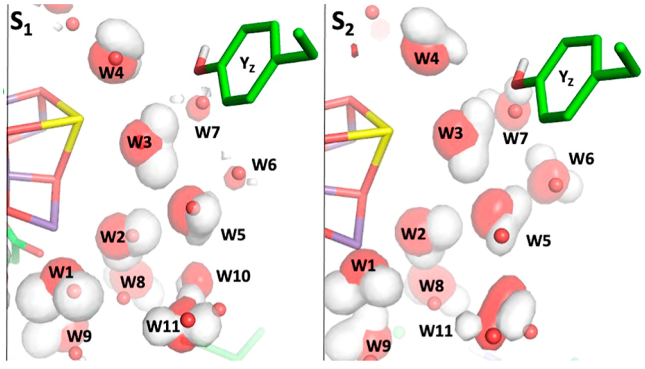

Figure 6. MD-derived PDF maps near the Y_Z water tetramer in two MD simulations (S_1, left panel and S_2, right) contoured at 15σ.

https://doi.org/10.1021/acs.jpcb.3c05367
J. Phys. Chem. B XXXX, XXX, XXX−XXX

occupancies increased from 0.3 for W6 and W7 in the S_1 state to 0.5 in the S_2 state (Table S1). This observation suggests that the unoptimized parameters for this tetramer for MD simulations may be correlated with the movement of Cl^- during the MD simulations. The tetramer is connected to the broad channel through two hydrogen-bonding pathways. Both pathways begin at W5, the first being W5−W2/W8-Cl and then the second being W5−W11−W10−N181-Cl (Figure 6).

Water Molecules Occupying Binding Sites inside the Large Channel. Figure S3 shows the MD-derived PDF maps for the dominant equilibrium positions of water molecules in the large channel. Starting with W_Y, the large channel has two distinct branches. The main branch is large inside, in which water molecules interact with each other but not much with the surface residues of the protein, i.e., the surface is not very hydrophilic. In this case, the partially ordered water molecule structures resemble bulk water structure. As such, water molecules occupying the large channel are not dependent on the $S_1 \rightarrow S_2$ transition. Due to the reduced hydrophilicity of this channel, it is the most suitable pathway for the somewhat hydrophobic product O_2 to exit. At a low contouring level of 1σ, a large mass of oxygen density can be seen (Figure S3). This contrasts with the narrow and broad channels, which had many distinct equilibrium positions for water molecules, even at this low contouring level (Figure 4). Increasing the contour to 15σ, the PDF for water molecules occupying the large channel almost completely disappears, except for very few disjointed and smeared peaks (Figure S3). The first four largest peaks were aligned with the X-ray-observed water molecules, although the PDFs for both oxygen and hydrogen atoms were far less spherically symmetric than those of water molecules in the narrow and broad channels. Other smaller peaks in the large channel visible at 15σ of the PDFs also partially overlap with the crystallographic observed positions of water molecules in both the 0F and 1F structures,[51,54] and all the remaining other sporadic peaks do not overlap with the crystallographic water molecules.

Water molecules occupying the secondary or lesser branch of the large channel are much more organized than the main branch, including 10 water molecules with spherically symmetric PDFs for both oxygen and hydrogen atoms. In contrast to residues lining the hydrophobic surface of the main branch, there are six D1 asparagine residues (N191, N298, N301, N303, N322, and N325) on the hydrophilic surface of the lesser branch. Even at a contour of 1σ of the PDFs, the equilibrium positions for 10 water molecules are distinct, unlike those in the main branch of the channel. Although a highly structured water network could serve as a proton exit pathway, this lesser branch is not connected to the bulk solvent. This branch has a dead end for proton movement, terminated at D1-A318, with N303 and N322 forming a physical barrier between water molecules occupying this branch and the next nearest cluster of water molecules.

DISCUSSION

Our study investigates the structural and substrate water dynamics particularly focusing on the $S_1 \rightarrow S_2$ transition using the snapshots from the S_1 and S_2 state MD trajectories. One of the important observations is the formation of a well-oriented hydrogen-bonded chain in the narrow channel, which has led to the proposal that this channel is the proton exit channel.[60] However, protons are not lost from the OEC when the S_1 state is oxidized. Hence, this proposal requires further examination. The orientation of the hydrogen-bonded chain, with protons pointing in toward the OEC, may help to discourage the outward proton transport. It was proposed that some changes of the properties of the narrow channel could serve as a closely coupled apparent proton shuttle, as suggested by Sakashita et al.,[60] involving a much less organized channel as a possible water supply path. Our observations on MD properties of this channel could indeed provide some support for that proposal. However, we argue that the increasing vacancy of water positions in the S_2 state prevents the narrow channel from being a viable, low-energy proton pathway.

The benefit of involving the broad channel as a proton pathway is that the broad channel does not have vacancy sites that could block the proton transfer. On the other hand, the narrow channel has a single-filed network of water molecules, which could break the continuity of the channel whenever a vacancy appears, which we found as a universal MD property based on our occupancy analysis. The non-single-filed network of hydrogen-bonding interactions inside the broad channel offers multiple paths for a Grotthuss mechanism.[15]

During the $S_1 \rightarrow S_2$ transition, there was no apparent large loss of occupancies of water molecules occupying the broad channel, which differed from water molecules occupying the narrow channel. It is likely that the branched water network inside the broad channel enables all water molecules to share any loss in any site, which is unlikely for the single-filed network of water molecules inside the narrow channel. While there is a branched network inside the broad channel, it has a somewhat limited constricted site through W8 and W9, which could serve as reliable steppingstones for a proton exit (Figure 4). Beyond the water cluster, the broad channel extends to two negatively charged residues, D1-E65 and D2-E312, which provide a strong negative electrostatic potential for attracting any released proton from the OEC. In addition, the water molecules in the broad channel behave like a bulk solvent in which individual sites have no large occupancy, yet the overall water molecule density reaches the maximum of a bulk solvent. In addition, the electrostatic potential near the end of the broad channel having both D1-E65 and D2-E312 is more negative and thereby more conducive to proton transport than that at the end of the narrow channel.

When chloride is removed for enzymatic studies, the $S_2 \rightarrow S_3$ transition is predominantly inhibited, which leads to the proposal that the formation of a D2-K317−D1-D61 salt-bridge could block the proton exit.[61−63] When D2-K317 is mutated to an alanine, chloride dependence is lost.[31,64] However, both the D1-D61A and D2-K317A mutants retain significant oxygen activity. These observations point to two key facts concerning the function of the water molecules occupying the broad channel. First, D1-D61 is the gateway for proton exit connected to either the narrow or broad channel.[15,31] Second, D2-K317 is not just a polar residue that is restrained by Cl^- but serves as some structural and/or hydrogen-bonding purpose for the enhanced cycling efficiency of the OEC. The X-ray-observed Cl1 position on a much longer timescale could represent a relaxed state after a proton is removed from the OEC. W9 and other water molecules of the water cluster in the broad channel are still able to pass through these two charged residues, as shown in Figure 4C,D. One cannot exclude the possibility that a proton transfer process may be coupled with unidentified transient repositioning of some assistant groups, including the Cl^- ion.

https://doi.org/10.1021/acs.jpcb.3c05367
J. Phys. Chem. B XXXX, XXX, XXX−XXX

In the case of the large channel, there is no evidence of protons passing through the barrier formed by asparagines because the distance between the two nearest water molecules in the two clusters is ∼6 Å, too long for any sort of hydrogen bond. The only possibility of a proton passing this way would be through the tautomerization of D1-N298, as proposed.[65] However, asparagine is not a good end-point proton acceptor, while the carboxylates of aspartate and glutamate residues found along the broad channel would be much better. It remains to be determined whether the tautomerization event of D1-N298 can occur on longer timescale MD simulations. Furthermore, occupancy maps in the large channel show a large oxygen density corresponding to bulk water. This shows that the mobility of water molecules is high in the large channel, which is also observed by the XFEL studies.[18]

CONCLUSIONS

Crystallographers often assign water molecules with unit occupancy in individual electron density peaks, where the assigned water molecules are capable of forming hydrogen bonds with protein residues or with other ordered water molecules. Smaller peaks of water molecules are then adjusted by increased atomic *B*-factors during model refinement. Upon the analysis of PDFs for dynamic water molecules moving through water channels using MD simulations, we find that water molecules do not have the unit occupancy found in an ice lattice or some highly ordered water binding sites on proteins. The occupancies are less than the unit value. If one considers that the protein provides rigid binding sites for water molecules, these sites are not occupied during a significant fraction of time. Conversely, when these sites are not occupied by water molecules, residues associated with these sites are more dynamic than when they are occupied. Therefore, many vacant sites appear to exist in the structured water networks that provide a basis of water and protein dynamics. An overall fraction of vacancy is likely dependent on the hydration state of the proteins. This observation explains how oxygen or carbon monoxide molecules can be rapidly diffused unhindered on and off the heme iron of hemoglobin and myoglobin through highly structured water networks.[66]

Our occupancy analysis further reveals that water molecules occupying the first few sites of the narrow channel leading away from the OEC form a single-filed structure, although the orientation of the hydrogens pointing in toward the OEC would not favor the outward proton transfer in the S_1 state. Instead, the quantitative analysis of occupancy suggests a "vacancy-hopping" mechanism for water transport in the narrow channel. We also provide a structural and molecular dynamic basis for a water molecule occupying the W_X binding pocket formed by D1-S169 and D1-D61 as a potential water substrate that has been stripped of hydrogen-bonding interactions with the enzyme and with other bound water molecules and is ready to bind to the OEC once the OEC is further oxidized.

ASSOCIATED CONTENT

Supporting Information

The Supporting Information is available free of charge at https://pubs.acs.org/doi/10.1021/acs.jpcb.3c05367.

Code to create occupancy maps, scripts and Matlab code for generating plots, occupancy analysis for water molecules in broad channel, water tetramer, and large channel, topology file for Fe-heme, and MD parameters——partial charges, bond, and angle parameters for S_1 and S_2 states (PDF)

AUTHOR INFORMATION

Corresponding Author

Divya Kaur − *Department of Chemistry, Brock University, Catharines L2S 3A1 Ontario, Canada;* orcid.org/0000-0002-8844-7709; Email: dmatta@brocku.ca

Authors

Krystle Reiss − *Department of Chemistry, Yale University, New Haven, Connecticut 06520-8107, United States*

Jimin Wang − *Department of Molecular Biophysics and Biochemistry, Yale University, New Haven, Connecticut 06520-8114, United States;* orcid.org/0000-0002-4504-8038

Victor S. Batista − *Department of Chemistry, Yale University, New Haven, Connecticut 06520-8107, United States;* orcid.org/0000-0002-3262-1237

Gary W. Brudvig − *Department of Chemistry, Yale University, New Haven, Connecticut 06520-8107, United States;* orcid.org/0000-0002-7040-1892

M. R. Gunner − *Department of Physics, City College of New York, New York, New York 10031, United States*

Complete contact information is available at: https://pubs.acs.org/10.1021/acs.jpcb.3c05367

Notes

The authors declare no competing financial interest.

ACKNOWLEDGMENTS

The authors would like to thank Drs. Zhuoran Long, Willian Armstrong, Ke Yang, and Ms. Jinchan Liu for helpful discussions. D.K. acknowledges support by the Brock University start-up funds. We also acknowledge financial support from the U.S. Department of Energy, Office of Basic Energy Sciences, Division of Chemical Sciences grant DE-FG02-05ER15646 (G.W.B.), and DE-SC0001423 (V.S.B., M.R.G.).

REFERENCES

(1) Kern, J.; Renger, G. Photosystem II: Structure and Mechanism of the Water:Plastoquinone Oxidoreductase. *Photosynth. Res.* **2007**, *94* (2−3), 183−202.

(2) Umena, Y.; Kawakami, K.; Shen, J.-R.; Kamiya, N. Crystal Structure of Oxygen-Evolving Photosystem II at a Resolution of 1.9 Å. *Nature* **2011**, *473* (7345), 55−60.

(3) Vinyard, D. J.; Brudvig, G. W. Progress toward a Molecular Mechanism of Water Oxidation in Photosystem II. *Annu. Rev. Phys. Chem.* **2017**, *68* (1), 101−116.

(4) Yano, J.; Kern, J.; Sauer, K.; Latimer, M. J.; Pushkar, Y.; Biesiadka, J.; Loll, B.; Saenger, W.; Messinger, J.; Zouni, A.; Yachandra, V. K. Where Water Is Oxidized to Dioxygen: Structure of the Photosynthetic Mn_4Ca Cluster. *Science* **2006**, *314* (5800), 821−825.

(5) Oliver, T.; Kim, T. D.; Trinugroho, J. P.; Cordón-Preciado, V.; Wijayatilake, N.; Bhatia, A.; Rutherford, A. W.; Cardona, T. The Evolution and Evolvability of Photosystem II. *Annu. Rev. Plant Biol.* **2023**, *74* (1), 225−257.

(6) Blankenship, R. E.; Hartman, H. The Origin and Evolution of Oxygenic Photosynthesis. *Trends Biochem. Sci.* **1998**, *23* (3), 94−97.

(7) Lubitz, W.; Chrysina, M.; Cox, N. Water Oxidation in Photosystem II. *Photosynth. Res.* **2019**, *142*, 105−125.

(8) McEvoy, J. P.; Brudvig, G. W. Water-Splitting Chemistry of Photosystem II. *Chem. Rev.* **2006**, *106* (11), 4455−4483.
(9) Kok, B.; Forbush, B.; McGloin, M. Cooperation of Charges in Photosynthetic O_2 Evolution-I. A Linear Four Step Mechanism. *Photochem. Photobiol.* **1970**, *11* (6), 457−475.
(10) Cox, N.; Pantazis, D. A.; Neese, F.; Lubitz, W. Biological Water Oxidation. *Acc. Chem. Res.* **2013**, *46* (7), 1588−1596.
(11) Askerka, M.; Brudvig, G. W.; Batista, V. S. The O_2-Evolving Complex of Photosystem II: Recent Insights from Quantum Mechanics/Molecular Mechanics (QM/MM), Extended X-Ray Absorption Fine Structure (EXAFS), and Femtosecond X-Ray Crystallography Data. *Acc. Chem. Res.* **2017**, *50* (1), 41−48.
(12) Lavergne, J.; Junge, W. Proton Release during the Redox Cycle of the Water Oxidase. *Photosynth. Res.* **1993**, *38* (3), 279−296.
(13) Dau, H.; Haumann, M. Eight Steps Preceding O-O Bond Formation in Oxygenic Photosynthesis-a Basic Reaction Cycle of the Photosystem II Manganese Complex. *Biochim. Biophys. Acta* **2007**, *1767* (6), 472−483.
(14) Walker, J. E.; Lutter, R.; Dupuis, A.; Runswick, M. J. Identification of the Subunits of F1F0-ATPase from Bovine Heart Mitochondria. *Biochemistry* **1991**, *30* (22), 5369−5378.
(15) Kaur, D.; Zhang, Y.; Reiss, K. M.; Mandal, M.; Brudvig, G. W.; Batista, V. S.; Gunner, M. R. Proton Exit Pathways Surrounding the Oxygen Evolving Complex of Photosystem II. *Biochim. Biophys. Acta, Bioenerg.* **2021**, *1862* (8), 148446.
(16) Sakashita, N.; Watanabe, H. C.; Ikeda, T.; Saito, K.; Ishikita, H. Origins of Water Molecules in the Photosystem II Crystal Structure. *Biochemistry* **2017**, *56* (24), 3049−3057.
(17) Vassiliev, S.; Zaraiskaya, T.; Bruce, D. Exploring the Energetics of Water Permeation in Photosystem II by Multiple Steered Molecular Dynamics Simulations. *Biochim. Biophys. Acta, Bioenerg.* **2012**, *1817* (9), 1671−1678.
(18) Hussein, R.; Ibrahim, M.; Bhowmick, A.; Simon, P. S.; Chatterjee, R.; Lassalle, L.; Doyle, M.; Bogacz, I.; Kim, I.-S.; Cheah, M. H.; Gul, S.; de Lichtenberg, C.; Chernev, P.; Pham, C. C.; Young, I. D.; Carbajo, S.; Fuller, F. D.; Alonso-Mori, R.; Batyuk, A.; Sutherlin, K. D.; Brewster, A. S.; Bolotovsky, R.; Mendez, D.; Holton, J. M.; Moriarty, N. W.; Adams, P. D.; Bergmann, U.; Sauter, N. K.; Dobbek, H.; Messinger, J.; Zouni, A.; Kern, J.; Yachandra, V. K.; Yano, J. Structural Dynamics in the Water and Proton Channels of Photosystem II during the S_2 to S_3 Transition. *Nat. Commun.* **2021**, *12* (1), 6531.
(19) Bhowmick, A.; Hussein, R.; Bogacz, I.; Simon, P. S.; Ibrahim, M.; Chatterjee, R.; Doyle, M. D.; Cheah, M. H.; Fransson, T.; Chernev, P.; Kim, I.-S.; Makita, H.; Dasgupta, M.; Kaminsky, C. J.; Zhang, M.; Gätcke, J.; Haupt, S.; Nangca, I. I.; Keable, S. M.; Aydin, A. O.; Tono, K.; Owada, S.; Gee, L. B.; Fuller, F. D.; Batyuk, A.; Alonso-Mori, R.; Holton, J. M.; Paley, D. W.; Moriarty, N. W.; Mamedov, F.; Adams, P. D.; Brewster, A. S.; Dobbek, H.; Sauter, N. K.; Bergmann, U.; Zouni, A.; Messinger, J.; Kern, J.; Yano, J.; Yachandra, V. K. Structural Evidence for Intermediates during O_2 Formation in Photosystem II. *Nature* **2023**, *617* (7961), 629−636.
(20) Shen, J.-R. The Structure of Photosystem II and the Mechanism of Water Oxidation in Photosynthesis. *Annu. Rev. Plant Biol.* **2015**, *66*, 23−48.
(21) Ho, F. M.; Styring, S. Access Channels and Methanol Binding Site to the $CaMn_4$ Cluster in Photosystem II Based on Solvent Accessibility Simulations, with Implications for Substrate Water Access. *Biochim. Biophys. Acta, Bioenerg.* **2008**, *1777* (2), 140−153.
(22) Saito, K.; William Rutherford, A.; Ishikita, H. Energetics of Proton Release on the First Oxidation Step in the Water-Oxidizing Enzyme. *Nat. Commun.* **2015**, *6*, 8488.
(23) Doyle, M. D.; Bhowmick, A.; Wych, D. C.; Lassalle, L.; Simon, P. S.; Holton, J.; Sauter, N. K.; Yachandra, V. K.; Kern, J. F.; Yano, J.; Wall, M. E. Water Networks in Photosystem II Using Crystalline Molecular Dynamics Simulations and Room-Temperature XFEL Serial Crystallography. *J. Am. Chem. Soc.* **2023**, *145*, 14621−14635.
(24) Zaharieva, I.; Dau, H.; Haumann, M. Sequential and Coupled Proton and Electron Transfer Events in the $S_2 \rightarrow S_3$ Transition of Photosynthetic Water Oxidation Revealed by Time-Resolved X-Ray Absorption Spectroscopy. *Biochemistry* **2016**, *55* (50), 6996−7004.
(25) Suga, M.; Akita, F.; Yamashita, K.; Nakajima, Y.; Ueno, G.; Li, H.; Yamane, T.; Hirata, K.; Umena, Y.; Yonekura, S.; Yu, L.-J.; Murakami, H.; Nomura, T.; Kimura, T.; Kubo, M.; Baba, S.; Kumasaka, T.; Tono, K.; Yabashi, M.; Isobe, H.; Yamaguchi, K.; Yamamoto, M.; Ago, H.; Shen, J.-R. An Oxyl/Oxo Mechanism for Oxygen-Oxygen Coupling in PSII Revealed by an x-Ray Free-Electron Laser. *Science* **2019**, *366* (6463), 334−338.
(26) Ibrahim, M.; Fransson, T.; Chatterjee, R.; Cheah, M. H.; Hussein, R.; Lassalle, L.; Sutherlin, K. D.; Young, I. D.; Fuller, F. D.; Gul, S.; Kim, I.-S.; Simon, P. S.; de Lichtenberg, C.; Chernev, P.; Bogacz, I.; Pham, C. C.; Orville, A. M.; Saichek, N.; Northen, T.; Batyuk, A.; Carbajo, S.; Alonso-Mori, R.; Tono, K.; Owada, S.; Bhowmick, A.; Bolotovsky, R.; Mendez, D.; Moriarty, N. W.; Holton, J. M.; Dobbek, H.; Brewster, A. S.; Adams, P. D.; Sauter, N. K.; Bergmann, U.; Zouni, A.; Messinger, J.; Kern, J.; Yachandra, V. K.; Yano, J. Untangling the Sequence of Events during the $S_2 \rightarrow S_3$ Transition in Photosystem II and Implications for the Water Oxidation Mechanism. *Proc. Natl. Acad. Sci. U.S.A.* **2020**, *117* (23), 12624−12635.
(27) Li, H.; Nakajima, Y.; Nomura, T.; Sugahara, M.; Yonekura, S.; Chan, S. K.; Nakane, T.; Yamane, T.; Umena, Y.; Suzuki, M.; Masuda, T.; Motomura, T.; Naitow, H.; Matsuura, Y.; Kimura, T.; Tono, K.; Owada, S.; Joti, Y.; Tanaka, R.; Nango, E.; Akita, F.; Kubo, M.; Iwata, S.; Shen, J.-R.; Suga, M. Capturing Structural Changes of the S_1 to S_2 Transition of Photosystem II Using Time-Resolved Serial Femtosecond Crystallography. *IUCrJ* **2021**, *8* (3), 431−443.
(28) Hussein, R.; Ibrahim, M.; Bhowmick, A.; Simon, P. S.; Bogacz, I.; Doyle, M. D.; Dobbek, H.; Zouni, A.; Messinger, J.; Yachandra, V. K.; Kern, J. F.; Yano, J. Evolutionary Diversity of Proton and Water Channels on the Oxidizing Side of Photosystem II and Their Relevance to Function. *Photosynth. Res.* **2023**, *158*, 91−107.
(29) Gisriel, C. J.; Wang, J.; Liu, J.; Flesher, D. A.; Reiss, K. M.; Huang, H.-L.; Yang, K. R.; Armstrong, W. H.; Gunner, M. R.; Batista, V. S.; Debus, R. J.; Brudvig, G. W. High-Resolution Cryo-Electron Microscopy Structure of Photosystem II from the Mesophilic Cyanobacterium, Synechocystis Sp. PCC 6803. *Proc. Natl. Acad. Sci. U.S.A.* **2022**, *119* (1), No. e2116765118.
(30) Lee, J.; Cheng, X.; Swails, J. M.; Yeom, M. S.; Eastman, P. K.; Lemkul, J. A.; Wei, S.; Buckner, J.; Jeong, J. C.; Qi, Y.; Jo, S.; Pande, V. S.; Case, D. A.; Brooks, C. L.; MacKerell, A. D.; Klauda, J. B.; Im, W. CHARMM-GUI Input Generator for NAMD, GROMACS, AMBER, OpenMM, and CHARMM/OpenMM Simulations Using the CHARMM36 Additive Force Field. *J. Chem. Theory Comput.* **2016**, *12* (1), 405−413.
(31) Kaur, D.; Szejgis, W.; Mao, J.; Amin, M.; Reiss, K. M.; Askerka, M.; Cai, X.; Khaniya, U.; Zhang, Y.; Brudvig, G. W.; Batista, V. S.; Gunner, M. R. Relative Stability of the S_2 Isomers of the Oxygen Evolving Complex of Photosystem II. *Photosynth. Res.* **2019**, *141* (3), 331−341.
(32) Matta, D. Role of Protonation State Changes and Hydrogen Bonding Around the Oxygen Evolving Complex of Photosystem II, CUNY Academic Works, 2021. https://academicworks.cuny.edu/gc_etds/4159 (accessed Feb 1, 2021).
(33) Reiss, K. Computational Investigations of the Oxygen-Evolving Complex and Its Water Network, Yale University, 2021. https://elischolar.library.yale.edu/gsas_dissertations/397. (accessed June 24, 2022).
(34) Eastman, P.; Swails, J.; Chodera, J. D.; McGibbon, R. T.; Zhao, Y.; Beauchamp, K. A.; Wang, L.-P.; Simmonett, A. C.; Harrigan, M. P.; Stern, C. D.; Wiewiora, R. P.; Brooks, B. R.; Pande, V. S. OpenMM 7: Rapid Development of High Performance Algorithms for Molecular Dynamics. *PLoS Comput. Biol.* **2017**, *13* (7), No. e1005659.
(35) Agarwal, R. C. A New Least-Squares Refinement Technique Based on the Fast Fourier Transform Algorithm. *Acta Crystallogr.* **1978**, *34* (5), 791−809.

https://doi.org/10.1021/acs.jpcb.3c05367
J. Phys. Chem. B XXXX, XXX, XXX−XXX

(36) Ten Eyck, L. F. Efficient Structure-Factor Calculation for Large Molecules by the Fast Fourier Transform. *Acta Crystallogr.* **1977**, *33* (3), 486−492.
(37) Brünger, A. T. Free R Value: A Novel Statistical Quantity for Assessing the Accuracy of Crystal Structures. *Nature* **1992**, *355* (6359), 472−475.
(38) Winn, M. D.; Ballard, C. C.; Cowtan, K. D.; Dodson, E. J.; Emsley, P.; Evans, P. R.; Keegan, R. M.; Krissinel, E. B.; Leslie, A. G. W.; McCoy, A.; McNicholas, S. J.; Murshudov, G. N.; Pannu, N. S.; Potterton, E. A.; Powell, H. R.; Read, R. J.; Vagin, A.; Wilson, K. S. Overview of the CCP4 Suite and Current Developments. *Acta Crystallogr., Sect. D: Biol. Crystallogr.* **2011**, *67* (4), 235−242.
(39) Wang, J.; Skeens, E.; Arantes, P. R.; Maschietto, F.; Allen, B.; Kyro, G. W.; Lisi, G. P.; Palermo, G.; Batista, V. S. Structural Basis for Reduced Dynamics of Three Engineered HNH Endonuclease Lys-to-Ala Mutants for the Clustered Regularly Interspaced Short Palindromic Repeat (CRISPR)-Associated 9 (CRISPR/Cas9) Enzyme. *Biochemistry* **2022**, *61* (9), 785−794.
(40) Wang, J.; Shi, Y.; Reiss, K.; Allen, B.; Maschietto, F.; Lolis, E.; Konigsberg, W. H.; Lisi, G. P.; Batista, V. S. Insights into Binding of Single-Stranded Viral RNA Template to the Replication-Transcription Complex of SARS-CoV-2 for the Priming Reaction from Molecular Dynamics Simulations. *Biochemistry* **2022**, *61* (6), 424−432.
(41) Wang, J.; Shi, Y.; Reiss, K.; Maschietto, F.; Lolis, E.; Konigsberg, W. H.; Lisi, G. P.; Batista, V. S. Structural Insights into Binding of Remdesivir Triphosphate within the Replication-Transcription Complex of SARS-CoV-2. *Biochemistry* **2022**, *61* (18), 1966−1973.
(42) Shi, Y.; Wang, J.; Batista, V. S. Translocation Pause of Remdesivir-Containing Primer/Template RNA Duplex within SARS-CoV-2's RNA Polymerase Complexes. *Front. Mol. Biosci.* **2022**, *9*, 999291.
(43) Maschietto, F.; Qiu, T.; Wang, J.; Shi, Y.; Allen, B.; Lisi, G. P.; Lolis, E.; Batista, V. S. Valproate-Coenzyme A Conjugate Blocks Opening of Receptor Binding Domains in the Spike Trimer of SARS-CoV-2 through an Allosteric Mechanism. *Comput. Struct. Biotechnol. J.* **2023**, *21*, 1066−1076.
(44) Janson, G.; Paiardini, A. PyMod 3: A Complete Suite for Structural Bioinformatics in PyMOL. *Bioinformatics* **2021**, *37* (10), 1471−1472.
(45) Wang, J. Determination of Chemical Identity and Occupancy from Experimental Density Maps. *Protein Sci.* **2018**, *27* (2), 411−420.
(46) Emsley, P.; Lohkamp, B.; Scott, W. G.; Cowtan, K. Features and Development of Coot. *Acta Crystallogr., Sect. D: Biol. Crystallogr.* **2010**, *66* (4), 486−501.
(47) Wang, J.; Smithline, Z. B. Crystallographic Evidence for Two-Metal-Ion Catalysis in Human Pol *η*. *Protein Sci.* **2019**, *28* (2), 439−447.
(48) Wang, J.; Gisriel, C. J.; Reiss, K.; Huang, H.-L.; Armstrong, W. H.; Brudvig, G. W.; Batista, V. S. Heterogeneous Composition of Oxygen-Evolving Complexes in Crystal Structures of Dark-Adapted Photosystem II. *Biochemistry* **2021**, *60* (45), 3374−3384.
(49) MATLAB. R2020b.
(50) Wang, J.; Askerka, M.; Brudvig, G. W.; Batista, V. S. Crystallographic Data Support the Carousel Mechanism of Water Supply to the Oxygen-Evolving Complex of Photosystem II. *ACS Energy Lett.* **2017**, *2* (10), 2299−2306.
(51) Suga, M.; Akita, F.; Hirata, K.; Ueno, G.; Murakami, H.; Nakajima, Y.; Shimizu, T.; Yamashita, K.; Yamamoto, M.; Ago, H.; Shen, J.-R. Native Structure of Photosystem II at 1.95 Å Resolution Viewed by Femtosecond X-Ray Pulses. *Nature* **2015**, *517* (7532), 99−103.
(52) Retegan, M.; Krewald, V.; Mamedov, F.; Neese, F.; Lubitz, W.; Cox, N.; Pantazis, D. A. A Five-Coordinate Mn(IV) Intermediate in Biological Water Oxidation: Spectroscopic Signature and a Pivot Mechanism for Water Binding. *Chem. Sci.* **2016**, *7* (1), 72−84.
(53) Suga, M.; Akita, F.; Sugahara, M.; Kubo, M.; Nakajima, Y.; Nakane, T.; Yamashita, K.; Umena, Y.; Nakabayashi, M.; Yamane, T.; Nakano, T.; Suzuki, M.; Masuda, T.; Inoue, S.; Kimura, T.; Nomura, T.; Yonekura, S.; Yu, L.-J.; Sakamoto, T.; Motomura, T.; Chen, J.-H.; Kato, Y.; Noguchi, T.; Tono, K.; Joti, Y.; Kameshima, T.; Hatsui, T.; Nango, E.; Tanaka, R.; Naitow, H.; Matsuura, Y.; Yamashita, A.; Yamamoto, M.; Nureki, O.; Yabashi, M.; Ishikawa, T.; Iwata, S.; Shen, J.-R. Light-Induced Structural Changes and the Site of O = O Bond Formation in PSII Caught by XFEL. *Nature* **2017**, *543* (7643), 131−135.
(54) Kern, J.; Chatterjee, R.; Young, I. D.; Fuller, F. D.; Lassalle, L.; Ibrahim, M.; Gul, S.; Fransson, T.; Brewster, A. S.; Alonso-Mori, R.; Hussein, R.; Zhang, M.; Douthit, L.; de Lichtenberg, C.; Cheah, M. H.; Shevela, D.; Wersig, J.; Seuffert, I.; Sokaras, D.; Pastor, E.; Weninger, C.; Kroll, T.; Sierra, R. G.; Aller, P.; Butryn, A.; Orville, A. M.; Liang, M.; Batyuk, A.; Koglin, J. E.; Carbajo, S.; Boutet, S.; Moriarty, N. W.; Holton, J. M.; Dobbek, H.; Adams, P. D.; Bergmann, U.; Sauter, N. K.; Zouni, A.; Messinger, J.; Yano, J.; Yachandra, V. K. Structures of the Intermediates of Kok's Photosynthetic Water Oxidation Clock. *Nature* **2018**, *563* (7731), 421−425.
(55) Pokhrel, R.; McConnell, I. L.; Brudvig, G. W. Chloride Regulation of Enzyme Turnover: Application to the Role of Chloride in Photosystem II. *Biochemistry* **2011**, *50* (14), 2725−2734.
(56) Amin, M.; Pokhrel, R.; Brudvig, G. W.; Badawi, A.; Obayya, S. S. A. Effect of Chloride Depletion on the Magnetic Properties and the Redox Leveling of the Oxygen-Evolving Complex in Photosystem II. *J. Phys. Chem. B* **2016**, *120* (18), 4243−4248.
(57) Gisriel, C. J.; Zhou, K.; Huang, H.-L.; Debus, R. J.; Xiong, Y.; Brudvig, G. W. Cryo-EM Structure of Monomeric Photosystem II from Synechocystis Sp. PCC 6803 Lacking the Water-Oxidation Complex. *Joule* **2020**, *4* (10), 2131−2148.
(58) Cukierman, S. Et Tu, Grotthuss! And Other Unfinished Stories. *Biochim. Biophys. Acta, Bioenerg.* **2006**, *1757* (8), 876−885.
(59) Teeter, M. M. Water Structure of a Hydrophobic Protein at Atomic Resolution: Pentagon Rings of Water Molecules in Crystals of Crambin. *Proc. Natl. Acad. Sci. U.S.A.* **1984**, *81* (19), 6014−6018.
(60) Sakashita, N.; Ishikita, H.; Saito, K. Rigidly Hydrogen-Bonded Water Molecules Facilitate Proton Transfer in Photosystem II. *Phys. Chem. Chem. Phys.* **2020**, *22* (28), 15831−15841.
(61) Ono, T.; Zimmermann, J. L.; Inoue, Y.; Rutherford, A. W. EPR Evidence for a Modified S-State Transition in Chloride-Depleted Photosystem II. *Biochim. Biophys. Acta, Bioenerg.* **1986**, *851* (2), 193−201.
(62) Boussac, A.; Setif, P.; Rutherford, A. W. Inhibition of Tyrosine Z Photooxidation after Formation of the S_3-State in Calcium-Depleted and Chloride-Depleted Photosystem-II. *Biochemistry* **1992**, *31* (4), 1224−1234.
(63) Wincencjusz, H.; van Gorkom, H. J.; Yocum, C. F. The Photosynthetic Oxygen Evolving Complex Requires Chloride for Its Redox State $S_2 \rightarrow S_3$ and $S_3 \rightarrow S_0$ Transitions but Not for $S_0 \rightarrow S_1$ or $S_1 \rightarrow S_2$ Transitions. *Biochemistry* **1997**, *36* (12), 3663−3670.
(64) Pokhrel, R.; Service, R. J.; Debus, R. J.; Brudvig, G. W. Mutation of Lysine 317 in the D2 Subunit of Photosystem II Alters Chloride Binding and Proton Transport. *Biochemistry* **2013**, *52* (28), 4758−4773.
(65) Chrysina, M.; de Mendonça Silva, J. C.; Zahariou, G.; Pantazis, D. A.; Ioannidis, N. Proton Translocation via Tautomerization of Asn298 During the S_2-S_3 State Transition in the Oxygen-Evolving Complex of Photosystem II. *J. Phys. Chem. B* **2019**, *123* (14), 3068−3078.
(66) Nishihara, Y.; Sakakura, M.; Kimura, Y.; Terazima, M. The Escape Process of Carbon Monoxide from Myoglobin to Solution at Physiological Temperature. *J. Am. Chem. Soc.* **2004**, *126* (38), 11877−11888.

https://doi.org/10.1021/acs.jpcb.3c05367
J. Phys. Chem. B XXXX, XXX, XXX−XXX